Thermochimica Acta 662 (2018) 116–125

Contents lists available at ScienceDirect

Thermochimica Acta

journal homepage: www.elsevier.com/locate/tca

Influence of minor additions of Si on the crystallization kinetics of $Cu_{55}Hf_{45}$ metallic glasses

O. Lozada-Flores[a], I.A. Figueroa[a,*], G. Gonzalez[a], A.E. Salas-Reyes[b]

[a] Instituto de Investigaciones en Materiales, Universidad Nacional Autónoma de México, Circuito exterior, Ciudad Universitaria, Coyoacán, Ciudad de México, 04510, Mexico

[b] Departamento de Ingeniería Metalúrgica, Facultad de Química, Universidad Nacional Autónoma de México, Circuito exterior, Ciudad Universitaria, Coyoacán, Ciudad de México, 04510, Mexico

ARTICLE INFO

Keywords:
Crystallization kinetics
Metallic glasses
Differential scanning calorimetry (DSC)
Activation energy

ABSTRACT

By means of differential scanning calorimetry the effects of minor additions of silicon on the crystallization kinetics of $Cu_{55-x}Hf_{45}Si_x$ (x = 0, 0.5, 1.0 and 2.0 at.%) alloys were studied. In the non-isothermal crystallization mode, the Kissinger method was used to obtaining the apparent activation energies of glass transition and crystallization. The highest E_g, E_x and E_p experimental values were found at 0.5 at.% of silicon i.e. E_g = 897.20 kJ/mol, E_x = 516.41 kJ/mol and E_p = 490.22 kJ/mol. In the isothermal mode, the Johnson-Mehl-Avrami model was employed in order to determine the crystallization kinetics, whilst the activation energies were analyzed with the Arrhenius equation. The results showed that addition of Si affect the relative amount of the crystallized phases. For the sample with 0.5 at.% Si content the ternary HfCuSi crystalline phase was predominant whilst for the samples with more Si, binary $Cu_{10}Hf_7$ and Hf Si phases were more abundant.

1. Introduction

Cu-based metallic glasses are materials that present many unique properties compared with crystallized counterparts because of the lack of long-range order in the atomic structure. In specific, binary Cu-based metallic glasses do not follow the empirical rules for glass formation [1] because they are composed of only two constituent elements, therefore, the potential for dense random packing of atoms is lower than that achieved for multicomponent alloys. However, several binary and ternary compositions have been studied and characterized in order to understand the glass formation [2–4], crystallization kinetics [5–10] and mechanical properties [11,12] of these alloys. On the other hand, microalloying (usually < 2 at.%) has demonstrated to have substantial effects on the glass forming ability of a number of glassy alloys [13–15]. In particularly, small substitutions of silicon (Si) in the ternary $Cu_{55}Hf_{25}Ti_{20}$ alloy increased the glass forming ability, GFA (up to Si = 0.5 at.%) but then tends to decrease at Si = 0.7, 1.0 and 2.0 at.% (d_c = 6 mm, 4 mm and 1 mm, respectively). Nevertheless, these results showed that the parameters obtained from thermal analysis, such as the supercooled liquid region, ΔT_x, and the reduced glass transition temperature, T_{rg}, generally did not correlate well with GFA [16]. Besides, with the addition of 1 at.% Si, the super-cooled liquid region range increased from 30 K to 60 K, while maintaining the same critical glassy diameter, d_c (4 mm) [17]. Due to the above, the study of the effect of Si on the crystallization kinetics of metallic glasses is very important, as the microadditions of Si did enhanced the glass forming ability and thermal stability of several bulk metallic glasses. In order to study a possible correlation between the minor additions of Si and crystallization kinetics of $Cu_{55-x}Hf_{45}Si_x$ (where x = 0.5, 1 and 2 at.%) glassy alloy, in the present work, the crystallization kinetics were investigated by continuous and isothermal analysis by differential scanning calorimetry (DSC) to measure the kinetics parameters. Apparent activation energies of glass transition, E_g, onset and peak of crystallization, E_x and E_p were calculated by means of the Kissinger's model [18]. In case of the isothermal heating, a Johnson-Mehl-Avrami model was [19] applied in order to understand the thermal stability and nucleation and growth behavior as a function of the small amounts of Si.

2. Experimental procedures

$Cu_{55-x}Hf_{45}Si_x$ (x = 0, 0.5, 1.0 and 2.0 at.%) alloy ingots were prepared by arc melting mixtures of Cu (99.99% pure), Hf (99.8% pure) and Si (99.9998% pure). Arc melting was performed in a Ti-gettered "Compact Arc Melter MAM-1, Edmund Bühler" under a high purity argon atmosphere. In order to obtain good chemical homogeneity, each ingot was re-melted at least six times. The alloy compositions represents

* Corresponding author.
E-mail address: iafigueroa@unam.mx (I.A. Figueroa).

https://doi.org/10.1016/j.tca.2018.02.006
Received 11 October 2017; Received in revised form 14 February 2018; Accepted 14 February 2018
Available online 20 February 2018
0040-6031/

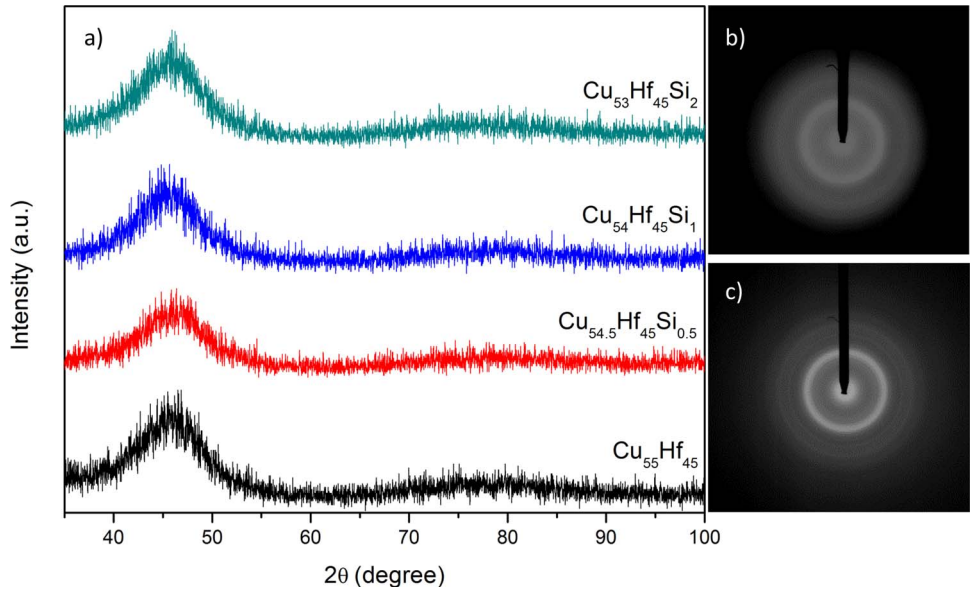

Fig. 1. a) XRD patterns of the ternary $Cu_{55-x}Hf_{45}Si_x$ (x = 0, 0.5, 1.0 and 2.0 at.%) alloys series, b) TEM diffraction patternd for the alloy $Cu_{55}Hf_{45}$ and c) TEM diffraction pattern for the $Cu_{53}Hf_{45}Si_2$ glassy alloy.

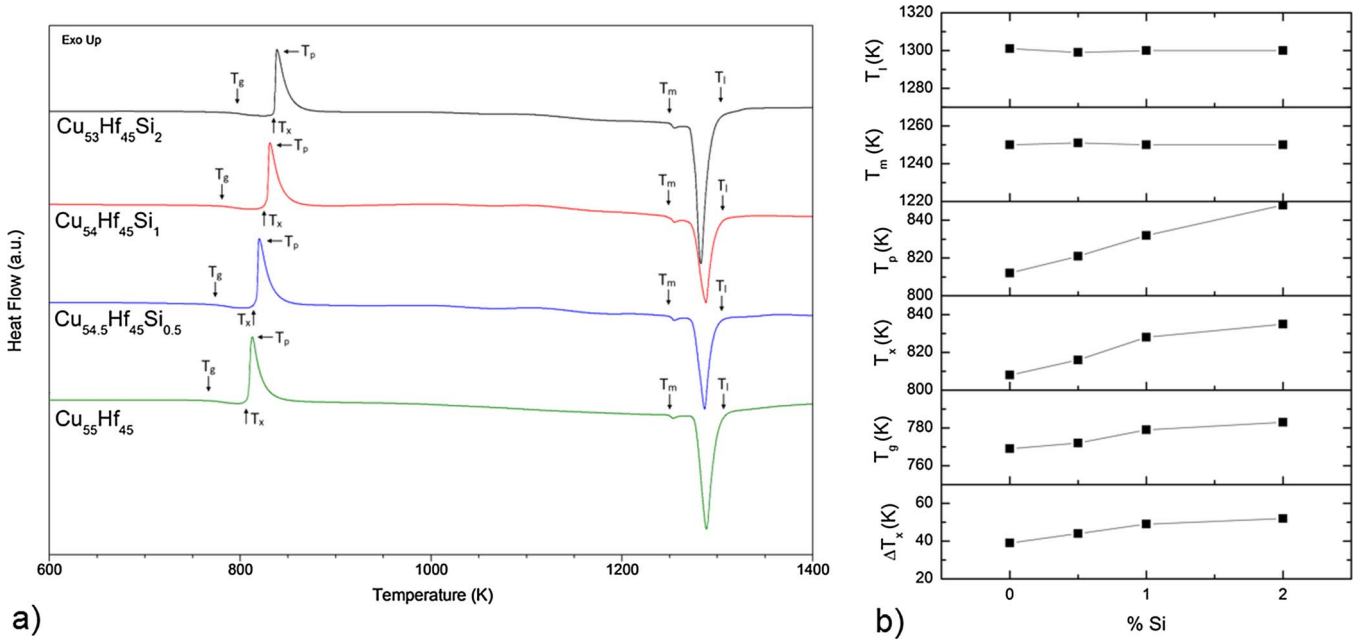

Fig. 2. DSC curves at continuous heating (20 K/min) for the investigated glassy alloys (a) and comparison between T_g, T_x, T_m, T_l and ΔT_x as a function of%Si (b).

nominal values thought the weight losses during melting were negligible (< 0.1%). Ribbon glassy samples were produced by chill-block melt spinning (Melt Spinner SC, Edmund Bühler) in a controlled helium atmosphere with an injection pressure of 0.4 bar, a nozzle orifice diameter of 0.8 mm and a tangential roll speed of 25 m/s. The gap between the crucible and the copper wheel was approximately 5 mm. The glass transition (T_g), the onset (T_x) and peak (T_p) temperatures of crystallization, *solidus* (T_m) and *liquidus* (T_l) temperatures (at a heating rate of 20 K/min) and the crystallization kinetics of the glassy samples were characterized by continuous and isothermal heating in a TA SDT Q600 calorimeter. Alumina sample holders and a constant flow of high purity Ar was used. The sample masses were approximately 60 mg.

In order to ensure the reliability of the data in the experiments, the SDT Q600 was calibrated, at the respective heating rates, using an indium standard specimen (T_m = 429.7 K) and zinc standard specimen (T_m = 692.6 K) giving an accuracy of ± 0.2 K and ± 0.02 mW. Dry N_2 and Ar were used as purge gases at a flow rate of 100 ml/min.

For the continuous heating, the heating rates applied were 5, 10, 20, 30 and 40 K/min up to 973 K. The isothermal crystallization experiments were performed in the super-cooled liquid region ($\Delta T_x = T_x - T_g$). Each sample was heated up to the annealing temperature at a heating rate of 20 K/min, then the samples were kept at the annealing temperature for a period of time until the crystallization is completed, after that, the samples were cooled down to room temperature. The DSC measurements were calibrated using a fresh zinc standard, giving an accuracy of ± 0.2 K and ± 0.02 mW. Additionally, in order to know which phases are formed when crystallization occurs, ribbons were cut and encapsulated in quartz under an Ar atmosphere. After this, they were subjected to an isothermal heat-treatment (within the ΔTx region) until the crystallization occurs. Structural characterization was examined by X-ray diffraction (XRD) using Co radiation (λ = 1.78897 Å)

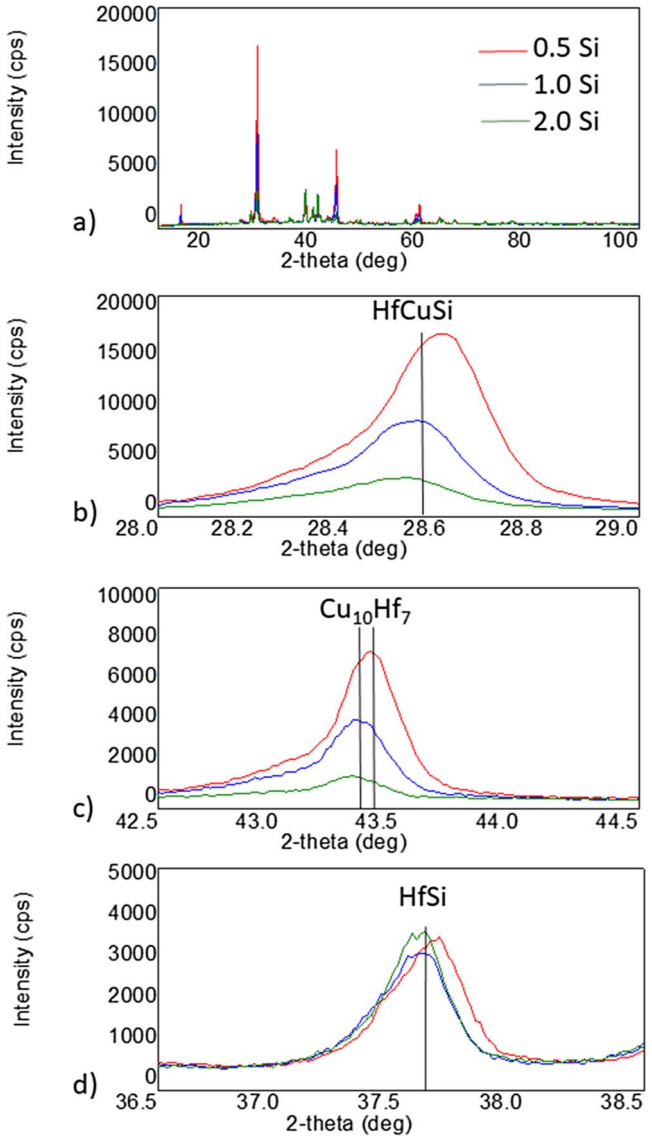

Fig. 3. Characteristic XRD from studied alloys a) whole pattern of $Cu_{55-x}Hf_{45}Si_x$ (where x = 0.5, 1.0 and 2.0 at.%) b) zoom from (002) Hf Cu Si phase, c) zoom from (313) and (133) Cu_{10} Hf_7 d) zoom from (111) Hf Si.

in a SIEMENS D-5000 diffractometer.

3. Results and discussion

The melt spun ribbons for the $Cu_{55-x}Hf_{45}Si_x$ (x = 0, 0.5, 1.0 and 2.0 at.%) alloys showed high metallic luster. The produced ribbon thickness was 28 μm ± 3, corresponding to the wheel speed of 25 m/s and could be easily bent through 180° without fracture. Fig. 1a shows the XRD patterns taken from the four glassy samples. These patterns showed rather wide peaks, indicating a fully glassy phase. On the other hand, Fig. 1b and c shows the electron diffraction pattern for the alloys $Cu_{55}Hf_{45}$ and $Cu_{53}Hf_{45}Si_2$, respectively. The XRD and TEM patterns demonstrated the glassy nature of the alloys studied.

Fig. 2 shows the DSC curves for the glassy samples at a heating rate of 20 K/min, indicating the crystallization peaks and temperature transitions. It can be noted that all DSC curves followed a typical behavior associated to metallic glasses: first, a glass transition point (T_g), followed by the ΔT_x zone and finally, the presence of the crystallization phenomena associated to the onset (T_x) and the peak (T_p) of the exhotermic curve. Additionally, the *solidus* (T_m) and *liquidus* (T_l) temperatures are also shown. On the other hand, a comparison between T_g, T_x, T_p, T_m, T_l and ΔT_x as a function of% Si are presented in Fig. 2b (all of these values were defined as the onset of endothermic and exothermic events). As observed in Fig. 2a, the addition of Si did not change the crystallization mode (showing one peak in DSC curve yet), however, it might either induce the formation of extra new phases for the final crystallization product or be preferentially dissolved in certain phases [14]. Based on the DSC scans, it can be seen that with the increment of the amount of Si microadditions, the super-cooled liquid region, ΔT_x, (a measure of glass thermal stability which is defined as the resistance of glasses towards devitrification upon reheating above T_g) increased, i.e. from 39 K to 58 K (Si = 0.0 and 2.0 at.%, respectively). This behavior is similar to previous reports in Cu-Hf-Ti system [16,17] where at Si = 0, 0.5, 1 and 2 at.%, the ΔT_x values were 25 K, 34 K, 53 K and 75 K, respectively. According to ref. [14] with the additions of Si, the liquid like structure is stabilized in the undercooled state due to that the small atoms can occupy interstitial spaces among the major constituent atoms, and this results in the increment of the packing density of the liquids.

The magnitude of T_g and T_x tended to increase as a function of Si content, from 769 K to 783 K for $Cu_{55}Hf_{45}$ and from 808 K to 835 K for $Cu_{53}Hf_{45}Si_2$. Therefore, the small additions of Si shifted the glass transition and crystallization events to higher temperatures, thus enlarging the super-cooled liquid region. It is important to note that the variations in the magnitude of T_x are higher than those for T_g.

The variation in T_p values could be explained in terms of the formation of new phases with the presence of Si (maintaining the same crystallization mode) or the change in the amount of such phases. From the XRD analysis (Fig. 3) of the heat-treated samples, it can be observed that the latter argument is the most plausible, as for the alloy with 0.5 at.% Si the main phase was HfCuSi. However, when the amount of Si increases the formation of different phases did increase i.e. $Cu_{10}Hf_7$ and Hf Si. It is important to note that the phase formed in the alloy with 0.5 is a ternary one, which in principle is more difficult to nucleate, explaining the reported glass formation of this alloy.

The parallel increase of T_x and T_p temperatures suggest that the amount of Si added to the binary alloy did move these points at higher temperatures, keeping the shape of the exothermic peak constant. Finally, it can be seen that the T_m and T_l values are almost constant, which implies that the small additions of Si did not affect these thermal parameters.

3.1. Non-isothermal crystallization analysis

Fig. 4 shows the DSC curves at heating rates of 5 k/min, 10 K/min, 20 K/min, 30 K/min and 40 K/min for a) $Cu_{55}Hf_{45}$, b) $Cu_{54.5}Hf_{45}Si_{0.5}$, c) $Cu_{54}Hf_{45}Si_1$ and d) $Cu_{53}Hf_{45}Si_2$ metallic glasses. It can be seen that all characteristic temperatures of the glassy alloys are shifted as the heating rate increases. This implies that T_g, T_x and T_p are dependent on the heating rate [20,21]. As can be seen, T_x is displaced to higher temperatures than T_g, this is because the crystallization involves diffusional processes over a longer range. On the other hand, these Cu-based metallic glasses showed one single stage of crystallization (one exothermic peak during DSC analysis). The values of T_g, T_x, T_p and ΔT_x as a function of heating rate are listed in Table 1.

From the DSC results, the apparent activation energy of the glass transition, crystallization and peak temperatures can be obtained, at different heating rates, using the Kissinger's equation [18]:

$$Ln\left(\frac{T^2}{\beta}\right) = \frac{E_a}{RT} + C \quad (1)$$

where β is the heating rate, R is the ideal gas constant and T is the specific temperature (T_g, T_x or T_p), E_a is the effective activation energy for glass transition and crystallization temperatures (T_g, T_x and T_p) and C is a constant. A plot of $Ln(T^2/\beta)$ vs $1000/T$ yields approximate straight lines, as shown in Fig. 5. From the slopes of these lines the

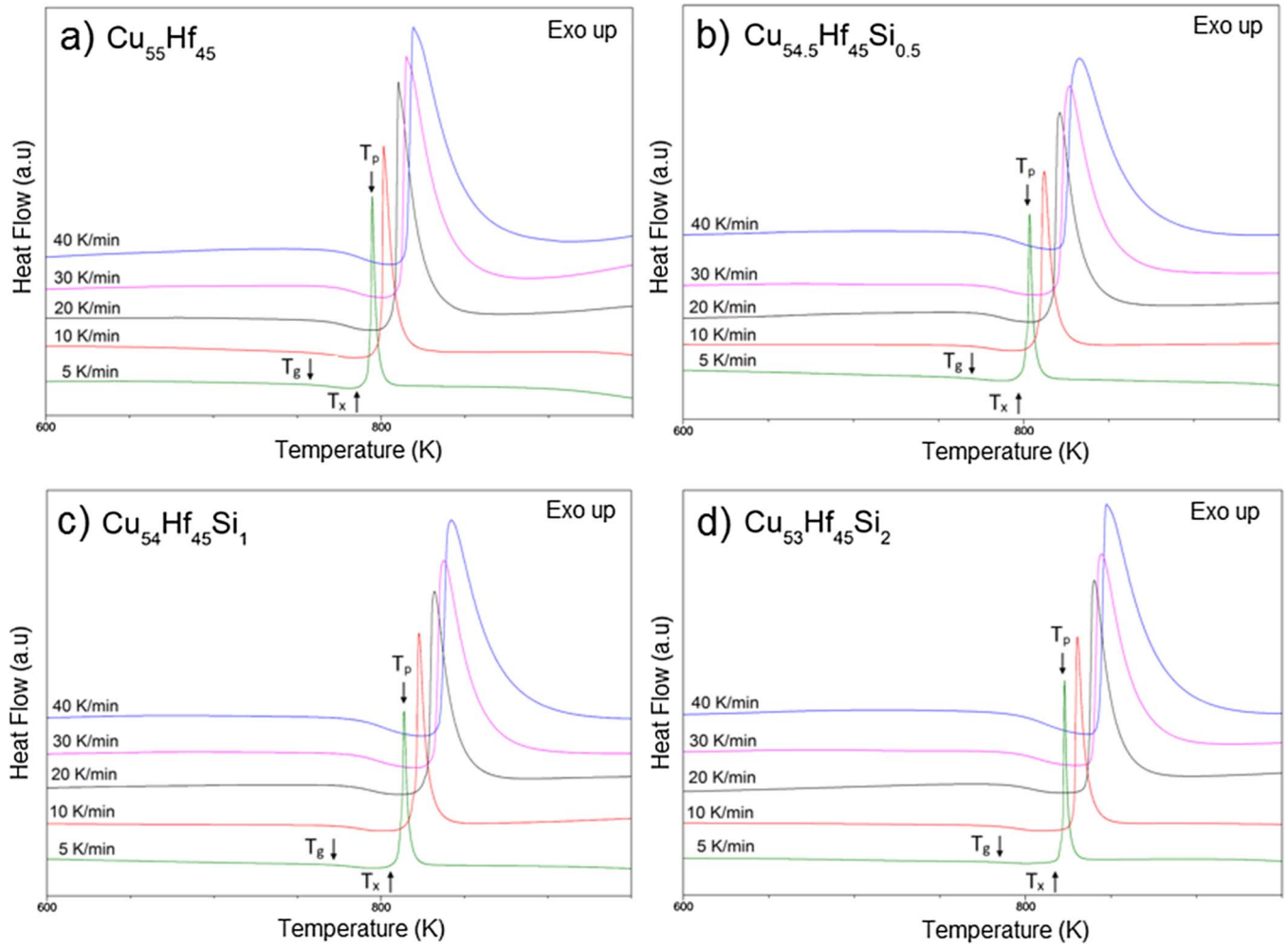

Fig. 4. DSC curves at heating rate of 5 K/min, 10 K/min, 20 K/min, 30 K/min and 40 K/min for a) $Cu_{55}Hf_{45}$, b) $Cu_{54.5}Hf_{45}Si_{0.5}$, c) $Cu_{54}Hf_{45}Si_1$ and d) $Cu_{53}Hf_{45}Si_2$ glassy alloys.

Table 1
Values of T_g, T_p, T_x, ΔT_x, E_g, E_x and E_p of glassy alloys studied.

Composition	Heating rate (K/min)	T_g (K)	T_x (K)	T_p (K)	ΔT_x (K)	E_g (kJ/mol)	E_x (kJ/mol)	E_p (kJ/mol)
$Cu_{55}Hf_{45}$	5	761	793	795	32	707.7	453.7	430.4
	10	765	800	803	35			
	20	769	808	812	39			
	30	773	813	817	40			
	40	775	817	820	42			
$Cu_{54.5}Hf_{45}Si_{0.5}$	5	765	801	806	36	879.2	516.4	490.2
	10	768	808	814	40			
	20	772	816	821	44			
	30	775	820	826	45			
	40	776	823	829	47			
$Cu_{54}Hf_{45}Si_1$	5	771	812	817	41	835.4	490.5	474.6
	10	774	821	825	47			
	20	779	828	832	49			
	30	781	832	837	51			
	40	783	836	842	53			
$Cu_{53}Hf_{45}Si_2$	5	774	824	823	47	811.5	483.9	459.8
	10	779	828	831	49			
	20	783	835	838	52			
	30	785	841	844	56			
	40	787	845	849	58			

activation energies were calculated.

Fig. 6 shows the obtained values of E_g, E_x and E_p as a function of % Si. For the $Cu_{55}Hf_{45}$ glassy alloy, the values of E_g, E_x and E_p were 707.7 kJ/mol, 453.7 kJ/mol and 430.4 kJ/mol, respectively. This results were very close to those we have previously reported [9], showing a rather good reproducibility. The value of E_g is higher than those for E_x and E_p, this behavior is the same in the four studied compositions, suggesting that the energetic barrier required for crystallization is less than that required for the glass transition. This implies that the atomic diffusion requires higher amounts of energy in glass transition than in

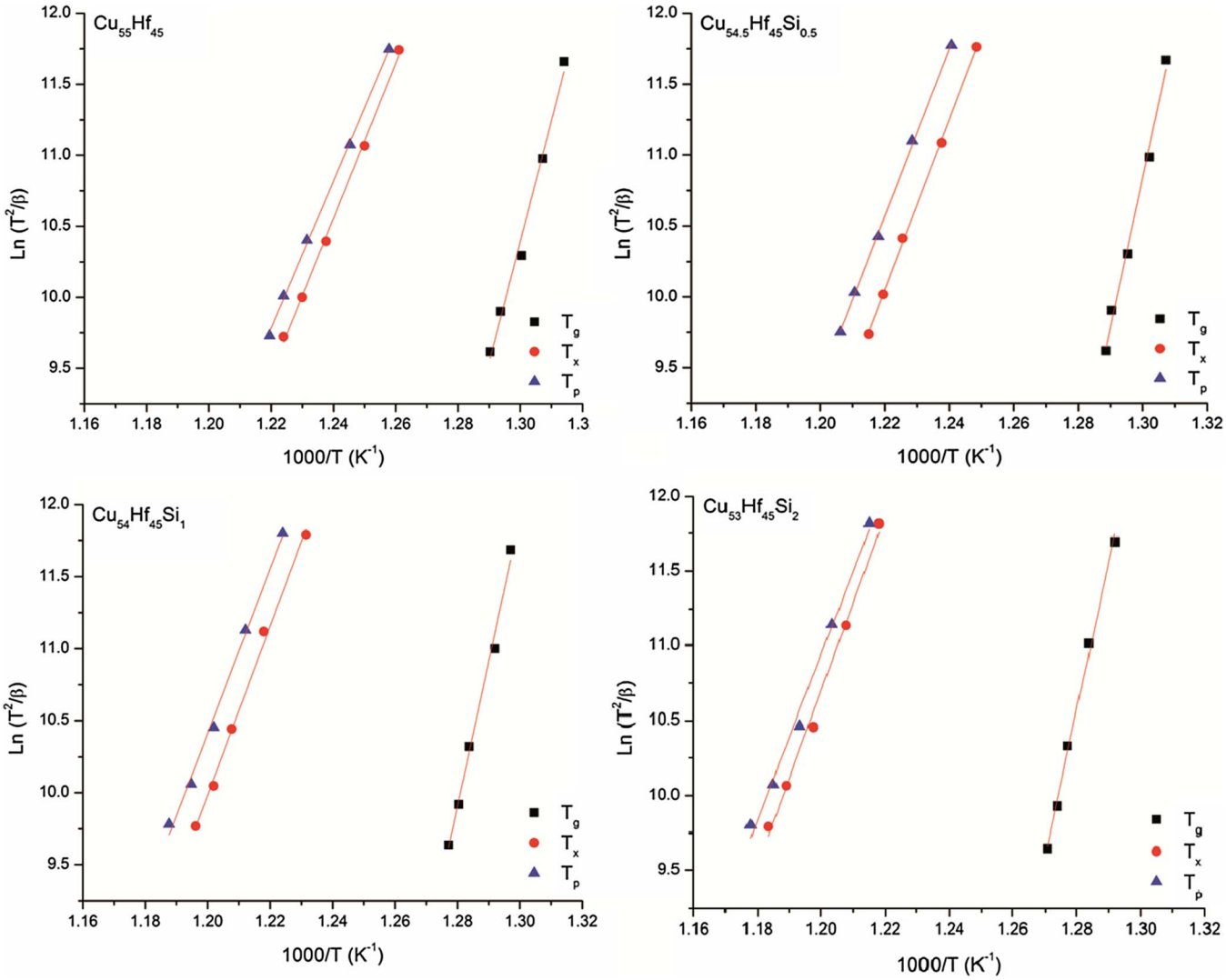

Fig. 5. Kissinger plots for $Cu_{55}Hf_{45}$, $Cu_{54.5}Hf_{45}Si_{0.5}$, $Cu_{54}Hf_{45}Si_1$ and $Cu_{53}Hf_{45}Si_2$ glassy alloys, from where E_g, E_x and E_p were calculated.

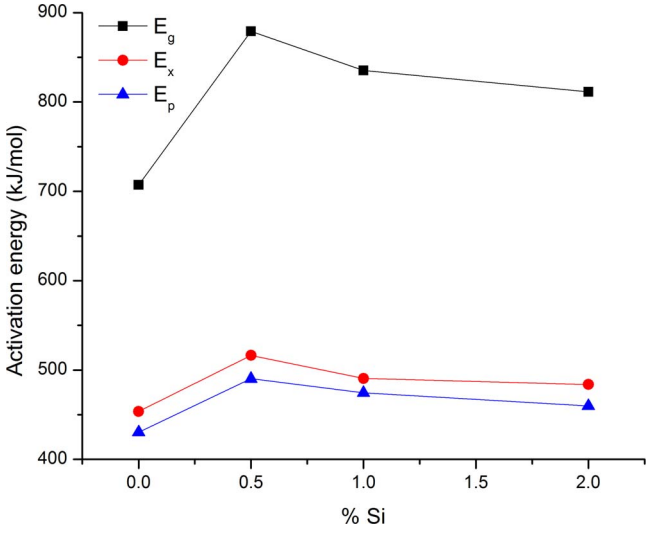

Fig. 6. Obtained values of E_g, E_x and E_p as a function of at.% Si.

the crystallization process to overcome the energy barrier and that the transformation takes place. On the other hand, the nucleation and grain growth are related to E_x and E_p [22], respectively. Therefore, the nucleation requires higher amount of energy than the grain growth process, as shown in Fig. 6. The values of E_g as a function of the at.% of Si were 707.7 kJ/mol, 879.2 kJ/mol, 835.4 kJ/mol and 811.5 kJ/mol for 0 at.%, 0.5 at.%, 1 at.% and 2 at.%, respectively. It can be seen that these values reached the maximum at 0.5 at.% Si and then went down to 2 at.% Si. The same behavior was also observed for E_x (E_x = 516.4 kJ/mol at 0.5 at.% Si) and E_p (E_p = 490.2 kJ/mol at 0.5 at.% Si). Since there is no correlation between ΔT_x (Fig. 2b) and the activation energies (Fig. 5); the magnitude of T_{rg} ($T_{rg} = T_g/T_l$) parameter was calculated for each alloy i.e., T_{rg} = 0.591, 0.594, 0.599 and 0.602 for x = 0, 0.5, 1 and 2, respectively. It is also worth mentioning that this semi-empiric parameter did not show a good correlation with the obtained apparent activation energies.

In the previous studies [16,17], the correlation between the small amounts of Si and GFA for $Cu_{55}Hf_{25}Ti_{20}$ metallic glass was studied. The results shows that the critical glassy diameters, d_c, obtained were 4 mm, 7 mm, 4 mm and 1 mm for $Cu_{55}Hf_{45}Ti_{20}$, $Cu_{54.5}$ $Hf_{45}Ti20Si_{0.5}$, $Cu_{54}Hf_{45}Ti_{20}Si_1$ and $Cu_{53}Hf_{45}Ti_{20}Si_2$, respectively. However, these d_c values did not correlate with "*post-mortem*" parameters obtained from thermal analysis (such as ΔT_x and T_{rg}), thus these parameters are unreliable indicators of GFA for, at least, these metallic glasses. Comparing the effect of Si on the GFA of the ternary $Cu_{55}Hf_{25}Ti_{20}$, and on the apparent activation energies of binary $Cu_{55}Hf_{45}$ glassy alloys, a good correlation can be observed between the d_c and E_g, E_x and E_p

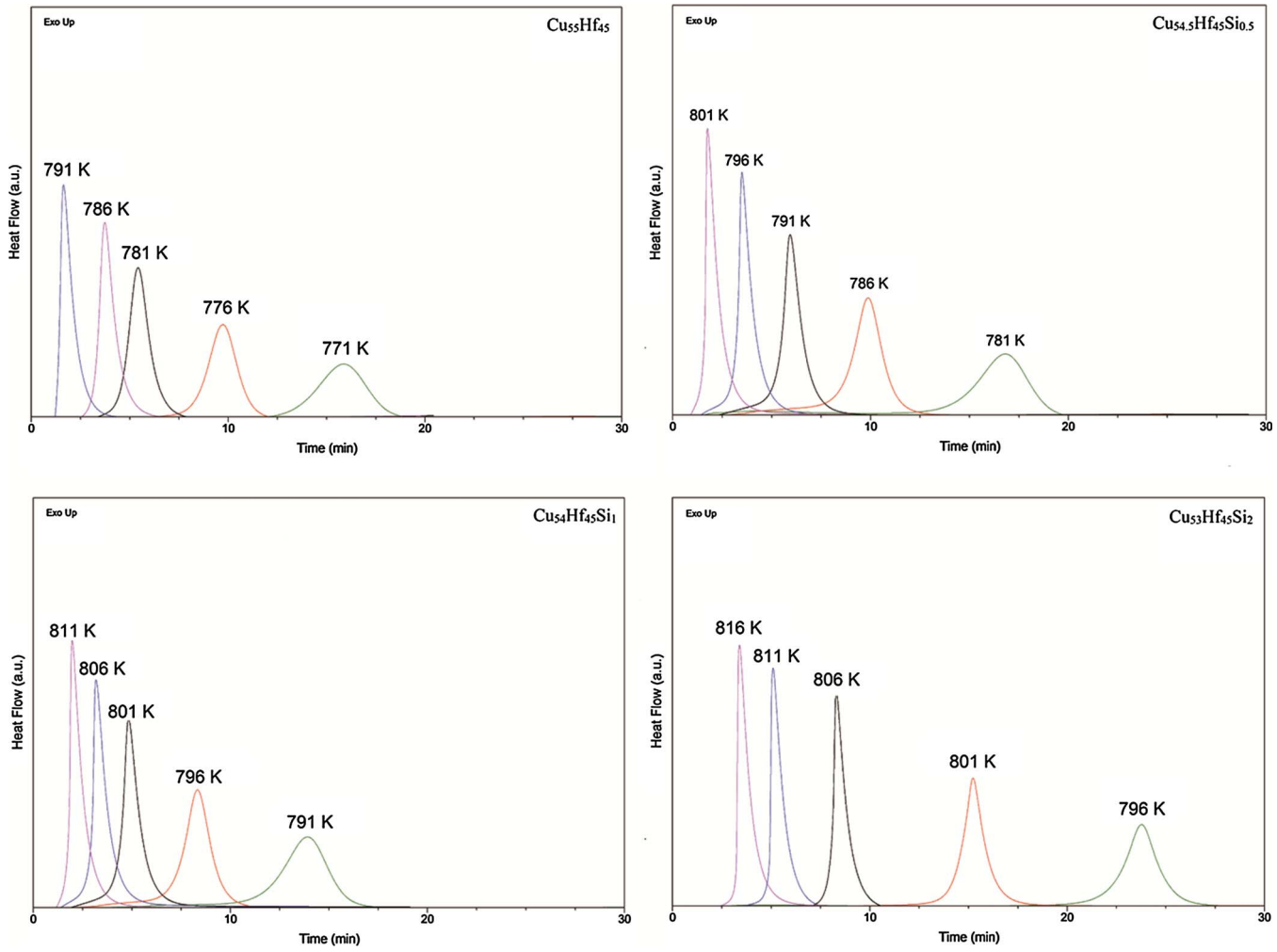

Fig. 7. DSC curves of studied metallic glasses.

values, in the range of x = 0 to 1. This could be explained due to the fact that the maximum values of d_c and energies corresponded to 0.5 at. % Si addition, and decreasing with higher amounts of such minor alloying element. Thus, the apparent activation energies could be used as a parameter of the GFA in binary Cu-Hf (and ternary Cu-Hf-Ti) metallic glasses.

3.2. Isothermal crystallization analysis

The isothermal analysis of $Cu_{55}Hf_{45}$ with small amounts of Si was carried out in the super-cooled liquid region, ΔT_x, at different annealing temperatures. It is noted that all the DSC curves (in isothermal annealing) exhibited a single exothermic peak after a certain incubation time, τ. This parameter is expressed as the time between the beginning of the crystallization and the required to reach the chosen annealing temperature. It can be seen that the crystallization is via "nucleation and growth" due to the fact that if higher annealing temperature is needed, the annealing time will be lower [23], as shown in Fig. 7.

To obtain the crystallized volume fraction as a function of annealing time, the following equation was used [24]:

$$\alpha(t) = \frac{A(t)}{A_\infty} \tag{2}$$

where A_∞ is the total area of the exothermic peak and A(t) is the partial area of the exothermic peak between the onset crystallization time and the chosen time. It can be noted that when increasing the annealing temperature (between T_g and T_x) the crystallization process is much faster. This could be attributed to the fact that at higher annealing temperatures, the atomic mobility is much higher. This behavior was the same for the four alloys studied (Fig. 8). Therefore, the minor additions of Si did not change the typical sigmoidal dependence with time, in these vitreous materials.

To study the isothermal crystallization kinetics of $Cu_{55-x}Hf_{45}Si_x$ (where x = 0, 0.5, 1 and 2), the Johnson-Melh-Avrami equation (JMA) [19,25] was used:

$$\alpha(t) = 1 - exp\{-[K(t-\tau)^n]\} \tag{3}$$

where n is the Avrami exponent, which is related to the characteristics of nucleation and growth during crystallization, τ is the incubation time and K is a reaction rate constant, related to the activation energy for the process. The values of K and n can be determined using the following relationship:

$$ln[-ln(1-\alpha(t))] = n\ lnK + n\ ln(t-\tau) \tag{4}$$

When plotting the $ln[-ln(1-\alpha(t))]$ *vs* $ln(t-\tau)$ for different temperatures, the JMA plots can be obtained and the Avrami exponent n and the reaction rate constant K can be calculated from the slope and intercept of the curves. Fig. 9 shows, for the crystallized fraction between 0.1 and 0.9, the JMA plots at the chosen annealing temperatures.

The average values were $n = 2.60$ for $Cu_{55}Hf_{45}$, $n = 2.58$ for $Cu_{54.5}Hf_{45}Si_{0.5}$, $n = 2.44$ for $Cu_{54}Hf_{45}Si_1$ and $n = 2.3$ for $Cu_{53}Hf_{45}Si_2$ glassy alloys. It can be noted that when increasing the amount of Si, the average value of n tends to decrease. These results are given in Table 2. It can be seen that when temperatures are close to T_g, the values of n

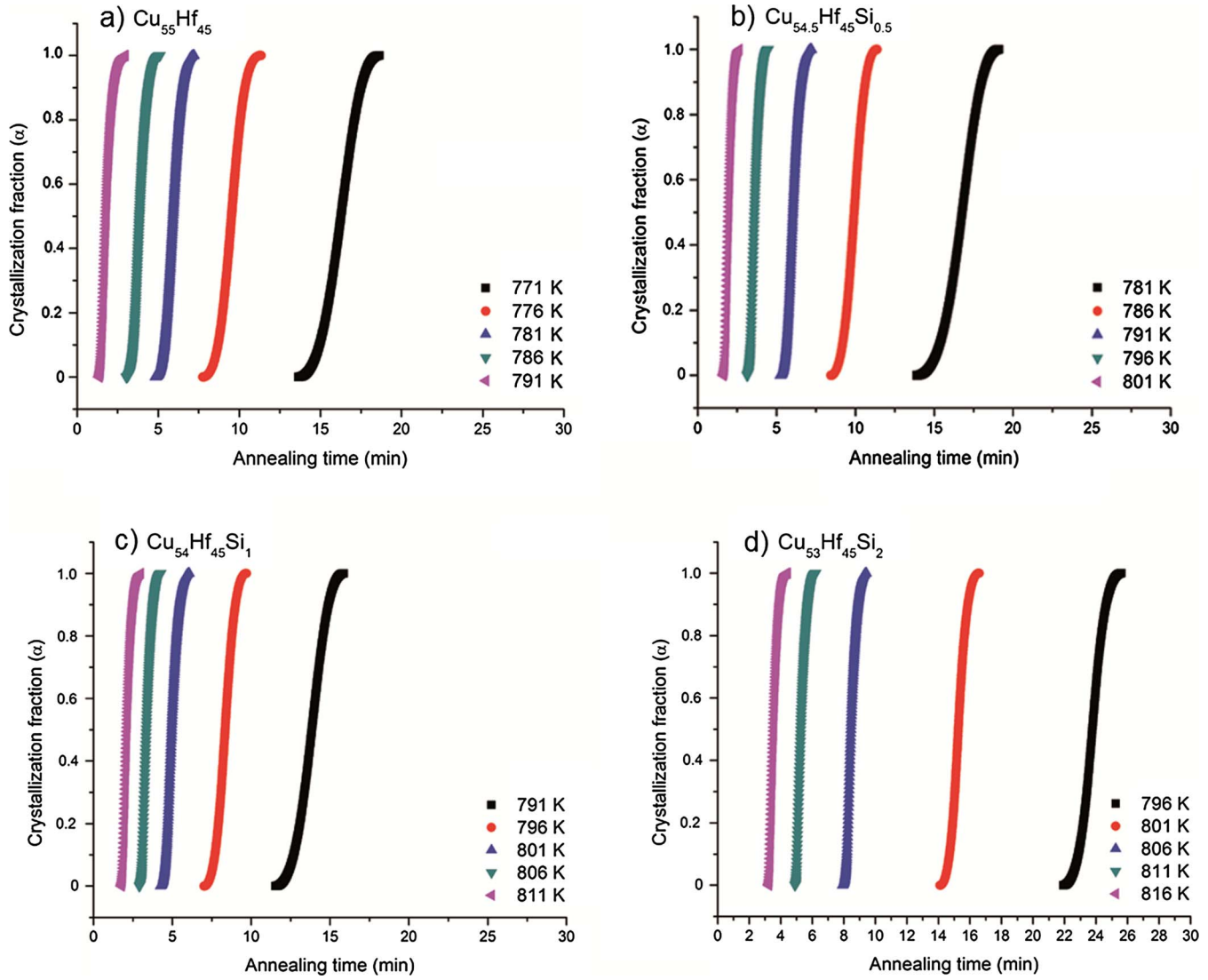

Fig. 8. Relationship between the crystallization fraction (α) and annealing time at different annealing temperatures for the studied Cu-based metallic glasses.

also drops. A plausible explanation of this can be given in terms of the annealing temperatures, since at lower annealing temperatures (near to T_g), the atomic diffusion is retarded, affecting the nucleation and growth (reducing the nucleation rate). Moreover, when the annealing temperature is near to T_x, the mobility of the atoms is relatively easy, promoting the increment of the nucleation rate.

It is known that the values of Avrami exponents are related to different crystallization transformation mechanism [26,27]: $n \approx 3$ implies a volume nucleation and two dimensional growth, with $n \approx 2$ there is a bulk nucleation and one dimensional growth. However, even though the obtained Avrami exponent's values have a tendency to increase as a function of at.% of Si, it is not possible to confirm that there is a change in the nucleation mechanism, since the variations in the average values on n values are less than 0.3. Therefore, additions of Si above 0.5 might change the crystallization kinetics (because at 0.5 at.% of Si, the maximum activation energies values were found).

The activation energy can be obtained by means of Arrhenius equation for the isothermal crystallization process using the relation between the time required, $t(\alpha)$, for a given crystallized fraction, α, and the annealing temperature [19]:

$$t(\alpha) = t_0 exp\left[\frac{E_c}{RT}\right] \quad (5)$$

where t_0 is a constant. Fig. 10 shows the approximate straight lines obtained by fitting the experimental values using the Arrhenius equation as a function of crystalline volume fractions (α = 0.1, 0.2, 0.3, 0.4, 0.5, 0.6, 0.7, 0.8 and 0.9). According to the slope of the straight lines, the average values of activation energy were 433 kJ/mol, 535 kJ/mol, 495 kJ/mol and 479 kJ/mol for the $Cu_{55}Hf_{45}$, $Cu_{54.5}Hf_{45}Si_{0.5}$, $Cu_{54}Hf_{45}Si_1$ and $Cu_{53}Hf_{45}Si_2$ glassy alloys, respectively. These values are very close to those obtained by means of continuous heating, implying that the crystallization follows a very similar phase transformation mechanism in isothermal and non-isothermal heating [28]. From this, the highest value of activation energy corresponds to 0.5 at.% Si and then tends to decrease as a function of the increment of Si in the alloys. It is important to point out that these values are higher than those for the binary $Cu_{55}Hf_{45}$ glassy alloy.

The activation energy as a function of crystallization volume fraction is shown in Fig. 11. For the studied alloys, the local activation energy decreased as the crystallized fraction increased, this is due to the fact that the activation energy consist in two main components: nucleation (related to T_x) and grain growth (relate to T_p). Initially, the activation energy values suggested the presence of a high-energy barrier. As the crystallization process takes place, the energy necessary for the nucleation decreases; therefore, the total value of the activation energy is low. However, as can be seen in Fig. 11, the local activation energies are high with the addition of 0.5 at.% Si and then tends to decrease to 2.0 at.% Si. This confirms that the activation energies

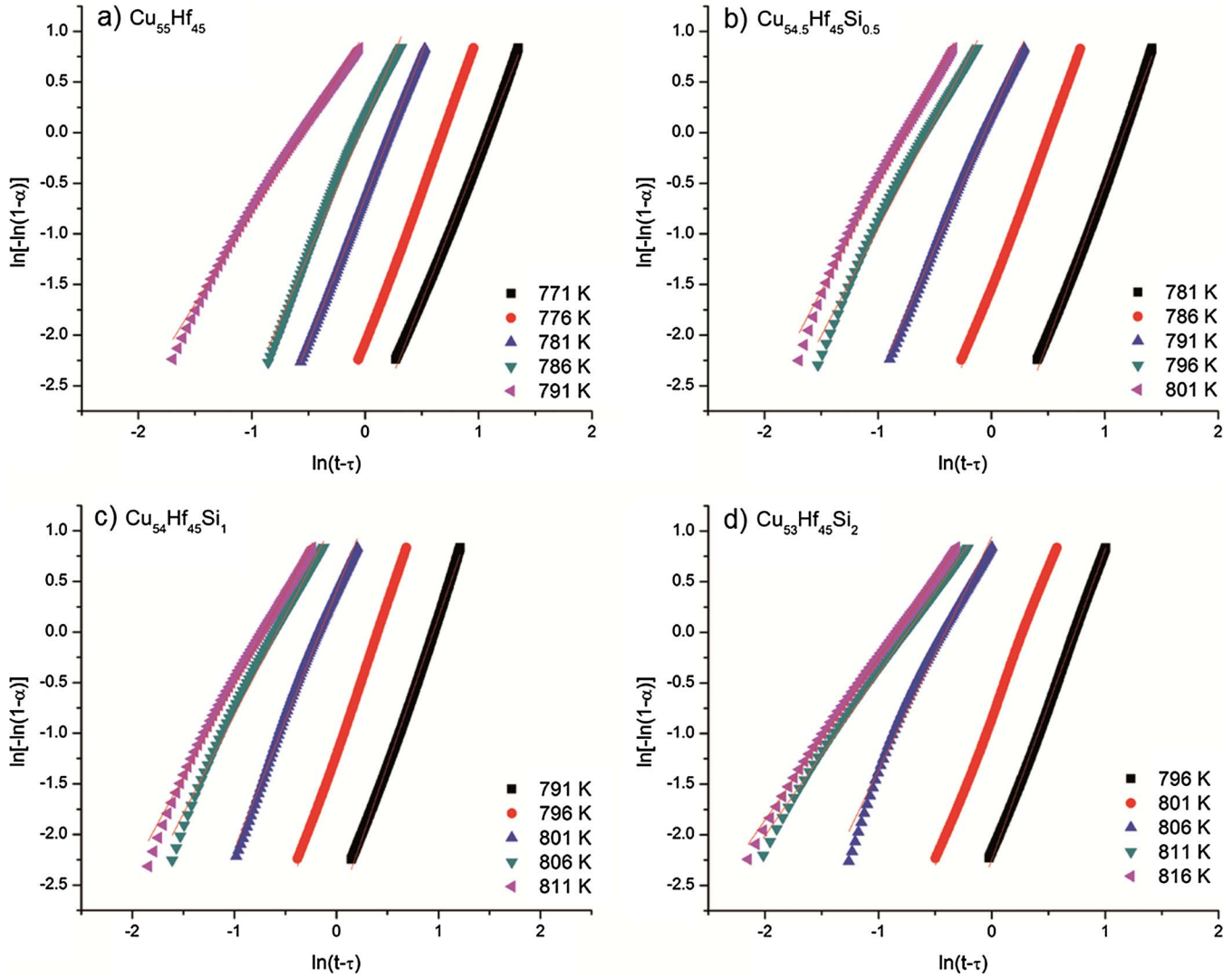

Fig. 9. JMA plots of the studied metallic glasses.

Table 2
Kinetic parameters for the glassy alloys studied.

Composition	Annealing temperature (K)	Incubation time, τ (min)	Avrami exponent, *n*	Reaction rate Constant, *K*
$Cu_{55}Hf_{45}$	771	13.77	2.84	0.33
	776	7.87	3.01	0.49
	781	4.92	2.82	0.79
	786	3.14	2.59	1.04
	791	1.42	1.72	1.77
$Cu_{54.5}Hf_{45}Si_{0.5}$	781	13.88	3.07	0.31
	786	8.44	2.98	0.60
	791	5.24	2.6	1.06
	796	3.13	2.12	1.74
	801	1.6	2.09	2.14
$Cu_{54}Hf_{45}Si_1$	791	11.54	2.92	0.39
	796	7.02	2.94	0.666
	801	4.24	2.56	1.17
	806	2.9	1.96	1.79
	811	1.75	1.83	2.04
$Cu_{53}Hf_{45}Si_2$	796	21.91	3.06	0.48
	801	14.1	2.96	0.76
	806	7.91	2.31	1.51
	811	4.91	1.61	2.10
	816	3.22	1.59	2.32

showed a good correlation with the GFA of the investigated Cu-based metallic glasses.

4. Conclusions

The crystallization kinetics of $Cu_{55}Hf_{45}$, $Cu_{54.5}Hf_{45}Si_{0.5}$, $Cu_{54}Hf_{45}Si_1$ and $Cu_{53}Hf_{45}Si_2$ glassy alloys and the effects of microaditions of Si were studied by means of differential scanning calorimetry under isothermal and continuous heating. Under continuous heating the obtained activation energies were determinate according to the Kissinger's model. In case of the $Cu_{55}Hf_{45}$ alloy, the obtained values were E_g = 707.18 kJ/mol, E_x = 453.70 kJ/mol and E_p = 430.44 kJ/mol, according to our previous report. On the other hand, the highest E_g, E_x and E_p values were obtained at 0.5 at.% of Si, i.e. E_g = 897.20 kJ/mol, E_x = 516.41 kJ/mol and E_p = 490.22 kJ/mol. The lowest activation energies values were found with the addition of 2.0 at.% of Si (E_g = 811 kJ/mol, E_x = 483 kJ/mol and E_p = 459 kJ/mol). These results indicated that the alloy with 0.5 at.% of Si has the highest thermal stability, and the alloy with 2.0 at.% of Si the easiest to vitrify. The activation energy reached its maximum values at 0.5 at.% of Si and then tended to drop. The average values of the obtained Avrami exponents, under isothermal conditions, were n = 2.60, n = 2.58, n = 2.44 and n = 2.3 for the $Cu_{55}Hf_{45}$, $Cu_{54.5}Hf_{45}Si_{0.5}$, $Cu_{54}Hf_{45}Si_1$ and $Cu_{53}Hf_{45}Si_2$ alloys, respectively. It was found that the crystallization

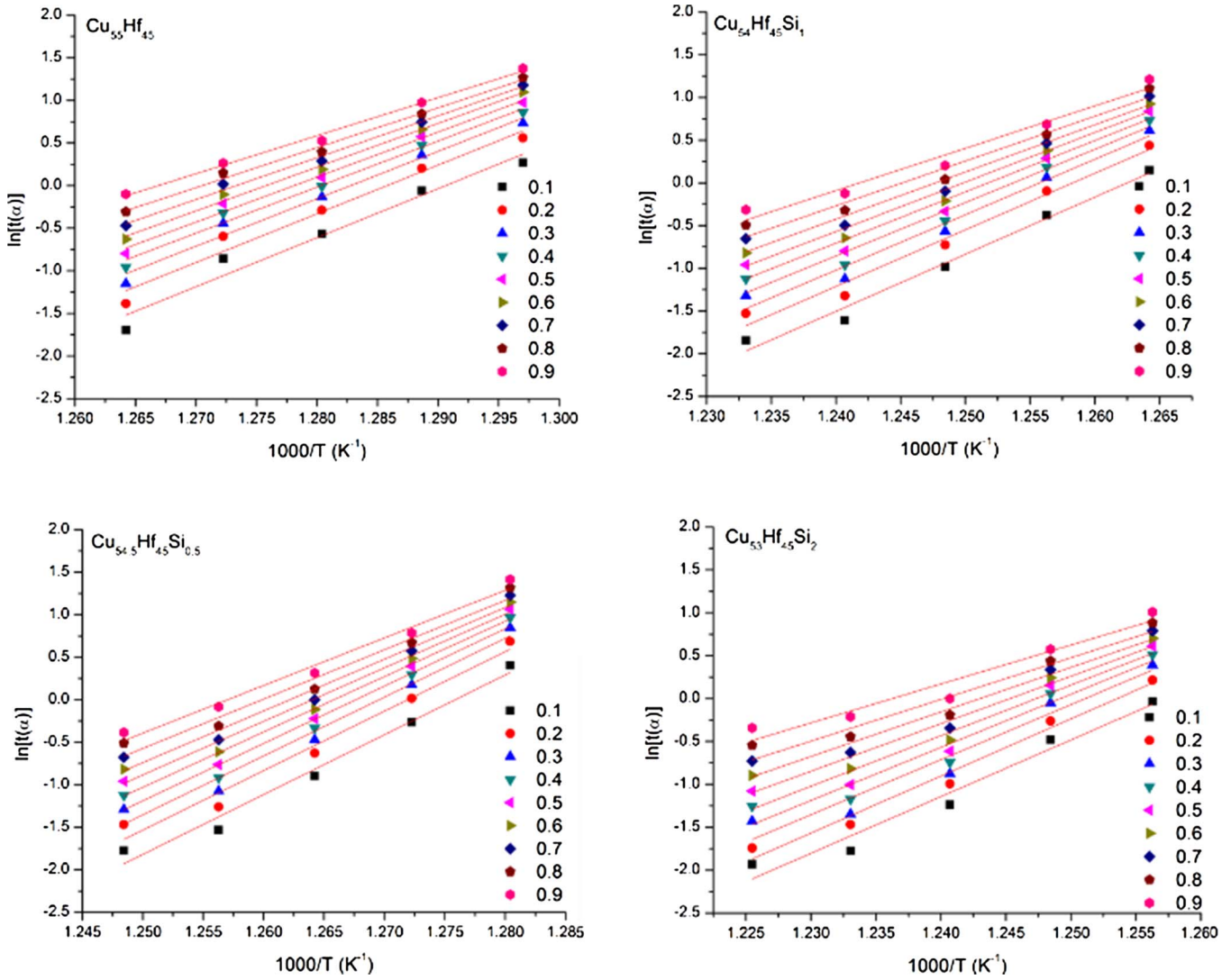

Fig. 10. Determination of the activation energy as a function of the different crystalline volume fractions, α, for the studied alloys.

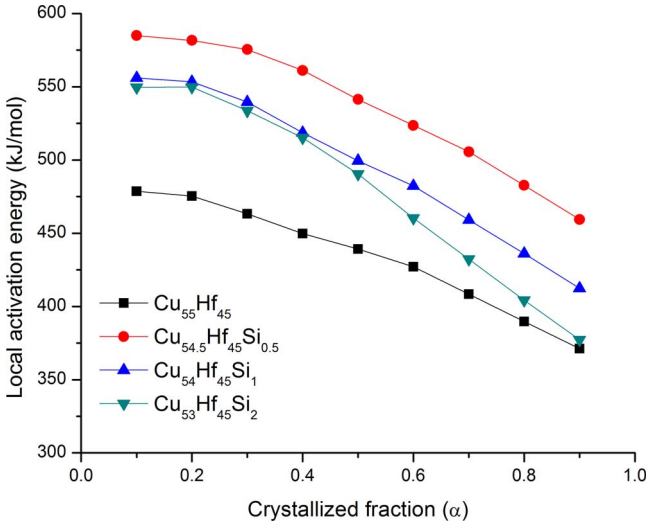

Fig. 11. Local activation energy as a function of crystallized volume fraction for the studied metallic glasses.

did change with Si additions above 0.5 at.%. The ternary HfCuSi crystalline phase was predominant for the alloy with 0.5 at.% Si, while the binary $Cu_{10}Hf_7$ and Hf Si phases were mainly detected for the alloys with 1 and 2 at.% Si.

Acknowledgements

The authors are grateful for the financial support of UNAM-DGAPA-PAPIIT through grant No. IN101016. A. Tejeda, O. Novelo, G. A. Lara, F. García, A. López-Vivas, C. Flores Morales, J. M. García, F. Silvar and C. Ramos are also acknowledged for their valuable technical support. "Por mi raza hablará el espíritu".

References

[1] A. Inoue, T. Zhang, T. Masumoto, Glass-forming ability of alloys, J. Non-Cryst. Solids 156–158 (2) (1993) 473–480.
[2] I.A. Figueroa, J.D. Plummer, G.A. Lara-Rodriguez, O. Novelo-Peralta, I. Todd, Metallic glass formation in the binary Cu–Hf system, J. Mater. Sci. 48 (2013) 1819–1825.
[3] G. Duan, D. Xu, W.L. Johnson, High copper content bulk glass formation in bimetallic Cu-Hf system, Metall. Mater. Trans. A 36 (2005) 455–458.
[4] L. Xia, D. Ding, S.T. Shan, Y.D. Dong, The glass forming ability of Cu-rich Cu-Hf binary alloys, J. Phys. Condens. Matter 18 (2006) 3543–3548.
[5] Q. Gao, Z. Jian, J. Xu, M. Zhu, F. Chang, A. Han, Crystallization kinetics of the $Cu_{50}Zr_{50}$ metallic glass under isothermal conditions, J. Solid State Chem. 244 (2016) 116–119.
[6] I. Kalay, M.J. Kramer, R.E. Napolitano, Crystallization kinetics and phase transformation mechanisms in $Cu_{56}Zr_{44}$ glassy alloy, Metall. Mater. Trans. A 46 A (2015) 3356–3364.
[7] A. Pratap, K.N. Lad, T.L.S. Rao, P. Majmudar, N.S. Saxena, Kinetics of crystallization

of amorphous $Cu_{50}Ti_{50}$ alloy, J. Non-Cryst. Solids 345–346 (2004) 178–181.
[8] S.T. Shan, L. Xia, D. Ding, Y.D. Dong, Thermal stability and kinetics of binary $Cu_{65}Hf_{35}$ bulk metallic glass, Chin. Phys. Lett. 23 (11) (2006) 3101–3104.
[9] O. Lozada-Flores, I.A. Figueroa, G.A. Lara, G. Gonzalez, C. Borja-Soto, J.A. Verduzco, Cryztallization kinetics of $Cu_{55}Hf_{45}$ glassy alloy, J. Non-Cryst. Solids 460 (2017) 1–5.
[10] I.A. Figueroa, H.A. Davies, I. Todd, Formation of Cu-Hf-Ti bulk metallic glasses, J. Alloys Compd. 434–435 (2007) 164–166.
[11] C.E. Borja-Soto, I.A. Figueroa, J.R. Fonseca, G.A. Lara-Rodriguez, J.A. Verduzco, Composition, elastic property and packing efficiency predictions for bulk metallic glasses in binary, ternary and quaternary systems, Mater. Res. 19 (2) (2016) 285–294.
[12] A. Inoue, W. Zhang, Formation, thermal stability and mechanical properties of Cu-Zr and Cu-Hf binary glassy alloy rods, Mater. Trans. 45 (2) (2004) 584–587.
[13] T. Egami, Formation and deformation of metallic glasses: atomistic theory, Intermetallics 14 (2006) 882–887.
[14] Z.P. Lu, C.T. Liu, Role of minor alloying additions in formation of bulk metallic glasses: a review, J. Mater. Sci. 39 (2004) 3965–3974.
[15] Z.P. Lu, C.T. Liu, W.D. Porter, Role of yttrium in glass formation of Fe-based bulk metallic glasses, Appl. Phys. Lett. 83 (13) (2003) 2581–2583.
[16] I.A. Figueroa, H.A. Davies, I. Todd, High glass formability for Cu–Hf–Ti alloys with small additions of Y and Si, Philos. Mag. 89 (27) (2009) 2355–2368.
[17] I.A. Figueroa, H.A. Davies, I. Todd, K. Yamada, Formation and thermal stability of Cu-Hf-Ti-M glassy alloys, Adv. Eng. Mater. 9 (6) (2007) 496–499.
[18] H.E. Kissinger, Reaction kinetics in differential thermal analysis, Anal. Chem. 29 (1957) 1702–1706.
[19] M. Avrami, Kinetics of phase change. I general theory, J. Chem. Phys. 7 (1939) 1103–1112.
[20] H.E. Kissinger, Variation of peak temperature with heating rate in differential thermal analysis, J. Res. Nat. Bur. Stand. 57 (4) (1956) 217–221.
[21] E. Matsubara, T. Ichitsubo, K. Itoh, T. Fukunaga, J. Saida, N. Nishiyama, H. Kato, A. Inoue, Heating rate dependence of T_g and T_x in Zr-based BMGs with characteristic structures, J. Alloys Compd. 483 (2009) 8–13.
[22] H.R. Wang, Y.L. Gao, G.H. Min, X.D. Hui, Y.F. Ye, Primary crystallization in rapidly solidified $Zr_{70}Cu_{20}Ni_{10}$ alloy from supercooled liquid region, Phys. Lett. A 314 (2003) 81–87.
[23] L.C. Chen, F. Speapen, Calorimetric evidence for the quasicrystalline structure of 'amorphous' Al/transition metal alloys, Nature 336 (1988) 366–368.
[24] C.S. Ray, W.H. Huang, D.E. Day, Crystallization kinetics of a lithia–silica glass: effect of sample characteristics and thermal analysis measurement techniques, J. Am. Ceram. Soc. 74 (1) (1991) 60–66.
[25] W.A. Johnson, R.F. Mehl, Reaction kinetics in processes of nucleation and growth, Trans. Am. Inst. Min. Metall. Pet. Eng. 135 (1939) 416–422.
[26] S. Mahadevan, A. Giridhar, A.K. Singh, Calorimetric measurements on As-Sb-Se glasses, J. Non-Cryst. Solids 88 (1) (1986) 11–34.
[27] J.W. Christian, The Theory of Transformation in Metals and Alloys, Pergamon Press, Oxford, 1965.
[28] Y.D. Sun, P. Shen, Z.Q. Li, J.S. Liu, M.Q. Cong, M. Jiang, Kinetics of crystallization process of Mg-Cu-Gd based bulk metallic glasses, J. Non-Cryst. Solids 358 (2012) 1120–1127.